Preparation of Graphite-Coated Iron Nanoparticles Using Pulsed Laser Decomposition of $Fe_3(CO)_{12}$ and PPh_3 in Hexane

Enyi Ye,† Binghai Liu, and Wai Yip Fan*

Department of Chemistry, National University of Singapore, 3 Science Drive 3, Singapore 117543

Received March 12, 2007. Revised Manuscript Received May 18, 2007

Graphite-coated iron nanoparticles with high magnetization have been synthesized by 355 nm pulsed laser photodecomposition of triiron dodecacarbonyl $Fe_3(CO)_{12}$ in the presence of triphenylphosphine PPh_3. The iron particles have been found to be stable toward oxygen and strong mineral acids. The graphite shell surrounding the iron core has been shown to possess defects on its outer layers, rendering them suitable for functionalization. These superparamagnetic spherical nanoparticles show a high magnetization value of 103.9 emu/g, as indicated by SQUID measurements. We believe that the as-prepared graphite-coated iron nanoparticles have great potential in magnetic resonance imaging and other biomagnetic applications.

Introduction

Magnetic nanoparticles are of great interest and iron, one of the most abundant elements on earth, has excellent magnetic properties.[1] Fine iron has been investigated for many years, but it is also easily oxidized, rendering it difficult to study and inconvenient for practical applications.[2] In the past few years, a large number of reports has focused on magnetic iron oxide nanoparticles[3] instead, as well as their dispersions in various media.[4] However, compared to these oxides, iron still has the highest room-temperature saturation magnetization value and also a sufficiently high Curie temperature for the majority of practical applications.[5] These superb properties made the preparation of iron nanoparticles highly desirable. Since then, a few methods have been developed to synthesize iron nanoparticles. For example, thermal[6] and sonochemical[7] decomposition of iron carbonyl [$Fe(CO)_5$] as well as thermal decomposition of sufficiently reactive iron-containing organometallic compounds[8] have been employed as precursors. However, the iron nanoparticles still need to be protected against oxidation in order to maintain their unique properties. Efforts have been performed to protect the iron nanoparticles using polymer-,[9] silica-,[10] gold-,[11] and carbon-coating[12] methods. Among these, the carbon-coating method is most effective. However, most of these preparations carried out in the gas phase[13] or solid state[14] at high temperatures have produced particles in large indiscrete aggregations, usually outside the nanometer range rather than controllable individual nanoparticle sizes.

Recently, we have developed a method[15] to prepare metallic nanoparticles upon laser decomposition of a suitable organometallic species in organic solvents. The advantage of the method lies first in the choice of the organometallic species, where the metal itself is already present in the zero oxidation state, hence eliminating the need for a reducing agent in the synthesis. Second, nanoparticles could be prepared under room-temperature conditions using light or laser to induce the decomposition of nanoparticles. We report here a facile synthesis of highly magnetizable graphite-coated iron nanoparticles by visible pulsed laser decomposition of commercially available $Fe_3(CO)_{12}$ in the presence of triphenylphosphine (PPh_3) in hexane. To the best of our knowledge, this is the first report for preparation of graphite-coated iron nanoparticles in solution at room temperature. In this one-pot synthesis, iron cores with average diameter of 100 nm are first generated by the complete laser decomposition of the precursor. This is followed by the generation of graphite shells around the iron cores upon catalytic graphitization of the PPh_3 adsorbates.

* Corresponding author. E-mail: chmfanwy@nus.edu.sg. Fax: 65-67791691. Tel: 65-65166823.

† Present address: Institute of Materials Research and Engineering, 3 Research Link, Singapore 117602.

(1) Farrell, D.; Cheng, Y.; McCallum, R. W.; Sachan, M.; Majetich, S. A. *J. Phys. Chem. B* **2005**, *109*, 13409.
(2) Huber, D. L. *Small* **2005**, *1*, 482.
(3) (a) Redl, F. X.; Cho, K. S.; Murry, C. B.; O'Brien, S. *Nature* **2003**, *423*, 968. (b) Hyeon, T.; Lee, S. S.; Park, J.; Chung, Y.; Na, H. B.; *J. Am. Chem. Soc.* **2001**, *123*, 12798. (c) Rockenberger, J.; Scher, E. C.; Alivisatos, A. P.; *J. Am. Chem. Soc.* **1999**, *121*, 11595.
(4) (a) Sun, S.; Zeng, H.; Robinson, D. B.; Raous, S.; Rice, P. M.; Wang, S. X.; Li, G. *J. Am. Chem. Soc.* **2003**, *126*, 273. (b) Deng, H.; Li, X.; Peng, Q.; Wang, X.; Chen, J.; Li, Y. *Angew. Chem., Int. Ed.* **2005**, *44*, 2782.
(5) Lide, D. R. *CRC Handbook of Chemistry and Physics*, 82nd ed.; CRC Press: Boca Roton, FL, 2001.
(6) Farrell, D.; Majetich, S.; Wilcoxon, J. *J. Phys. Chem. B* **2003**, *107*, 11022.
(7) Suslick, K.; Fang, M.; Hyeon, T. *J. Am. Chem. Soc.* **1996**, *118*, 11960.
(8) Dumestre, F.; Chaudret, B.; Amiens, C.; Renaud, P.; Fejes, P. *Science* **2004**, *303*, 821.
(9) (a) Burke, N. A. D.; Stoever, H. D. H.; Dawson, F. P. *Chem. Mater.* **2002**, *14*, 4752. (b) Kuroda, C. S.; Maeda, M.; Nishibiraki, H.; Matsushita, N.; Handa, H.; Abe, M. *IEEE Trans. Magn.* **2005**, *40*, 4117.
(10) Tartaj, P.; Serna, C. J. *J. Am. Chem. Soc.* **2003**, *125*, 15754.
(11) Cho, S. J.; Idrobo, J. C.; Olamit, J.; Liu, K.; Browning, N. D.; Kauzlarich, S. M. *Chem. Mater.* **2005**, *17*, 3181.
(12) (a) Si, P. Z.; Zhang, Z. D.; Geng, D. Y.; You, C. Y.; Zhao, X. G.; Zhang, W. S. *Carbon* **2003**, *41*, 247; (b) Huo, J.; Song, H.; Chen, X. *Carbon* **2004**, *42*, 3177. (c) Ma, Y.; Hu, Z.; Huo, K.; Lu, Y.; Liu, J.; Chen, Y. *Carbon* **2005**, *43*, 1667.
(13) Díaz, L.; Santos, M.; Ballesteros, C.; Maryško, M.; Pola, J. *J. Mater. Chem.* **2005**, *15*, 4311.
(14) Hisato, T.; Shigeo, F.; Takeo, O. *J. Mater. Chem.* **2004**, *14*, 253.
(15) Ye, E.; Tan, H.; Li, S.; Fan, W. Y. *Angew. Chem., Int. Ed.* **2006**, *45*, 1120.

10.1021/cm0706797 CCC: $37.00
Published on Web 06/27/2007

Experimental Section

In a typical experiment, $Fe_3(CO)_{12}$ (5−10 mg, 99% Sigma-Aldrich) and PPh_3 (30−60 mg, 99% Sigma-Aldrich) with a P/Fe ratio of 1:20 were dissolved in 10−30 mL of deoxygenated hexane to form a green solution. This represented a concentration of 0.3 to 2.0 × 10^{-4} M for $Fe_3(CO)_{12}$ in hexane. The UV−visible absorption spectrum of this solution was recorded using a Shimadzu uv-2550 spectrometer to check for its absorptivity. The broad absorption spectrum ranging from 200 to 750 nm indicated that it is possible to induce photodecomposition of $Fe_3(CO)_{12}$ using a pulsed laser at $\lambda = 355$ nm. The solution was then irradiated by a 355 nm nanosecond pulsed YAG laser (Continuum Surelite III-10, ∼70 mJ/pulse, 10 ns pulse) under vigorous stirring for 2 h. Different laser energies per pulse have been attempted but small energies (<20 mJ/pulse) over the same time did not produce iron nanoparticles, whereas energies higher than 100 mJ/pulse tend to damage the flask. A change of color from green to brown occurred in about 10 min as $Fe_3(CO)_{12}$ decomposed, followed by another change from brown to black, which indicated the formation of iron clusters. The solution remained black upon further irradiation. The particles were collected by a magnet, rinsed with hexane several times, and then redispersed in hexane for further characterization. A drop of this suspension was put on the copper grid and allowed to dry in air for transmission electron microscopy (TEM) study.

Results and Discussion

We have varied the concentrations of $Fe_3(CO)_{12}$ from 1 × 10^{-5} to 1 × 10^{-4} M with a $Fe_3(CO)_{12}$:PPh_3 ratio of 1:20. The variation of the concentration is limited to the solubility of iron carbonyl in hexane. Iron as opposed to iron oxide nanoparticles can only be found at a $Fe_3(CO)_{12}$:PPh_3 ratio of about 4, beyond which no more significant changes are produced. High laser fluences were required and will be discussed later. However, there is a limit to the maximum laser energy to avoid damaging the glass container. It appears two different size distributions were observed where the larger iron nanoparticles ranged from 100 to 200 nm, whereas the smaller ones ranged from 20 to 30 nm. (see Figure 1).

Bright-field TEM images of the as-prepared graphite-coated iron particles taken with a JEOL JEM 2010F TEM instrument (200 keV) are shown in Figure 1. The core−shell nanostructures can be seen with the shell estimated to be around 10 nm thick. The graphite shells were more clearly seen in the bright-field TEM image (Figure 2a) at a higher magnification (JEOL JEM 3010 TEM, 300 keV). In the dark-field image (Figure 2b), the diffraction contrast of the graphite shell indicates that the iron core was fully coated with highly crystalline graphite. The high-resolution image of the graphite shell (Figure 2c) showed a lattice spacing of 0.34 nm, which corresponds to the (002) planes of crystalline graphite. It is worth pointing out that almost every iron particle, whether large (>100 nm) or small (<30 nm), was coated with a compact graphite shell. High-resolution TEM of the iron core (Figure 2d) was also taken, and from the image, it is seen that the core is composed of small-sized grains. Selected area electron diffraction (SAED) of these core−shell nanostructures (Figure 2e) showed a typical polycrystalline structure and the existence of graphite and body-centered cubic (bcc) iron, as evidenced by the lattice spacings of 0.34 nm corresponding to (002) of graphite, 0.202 nm to (110) of bcc iron, and 0.117 nm to (211) of bcc iron. The diffusive scattering in SAED indicates a rather small grain size of iron, consistent with the high-resolution TEM analysis in Figure 2d.

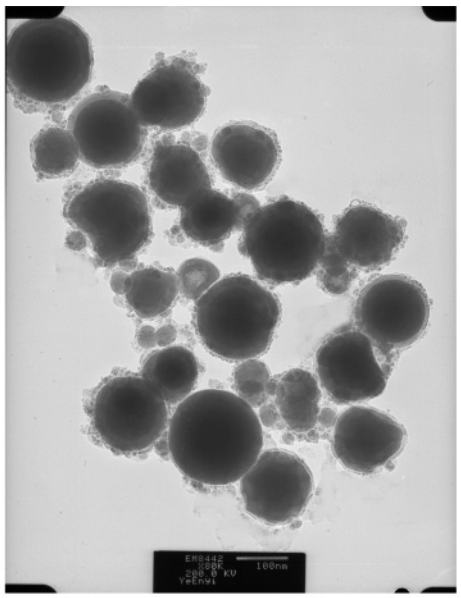

(a)

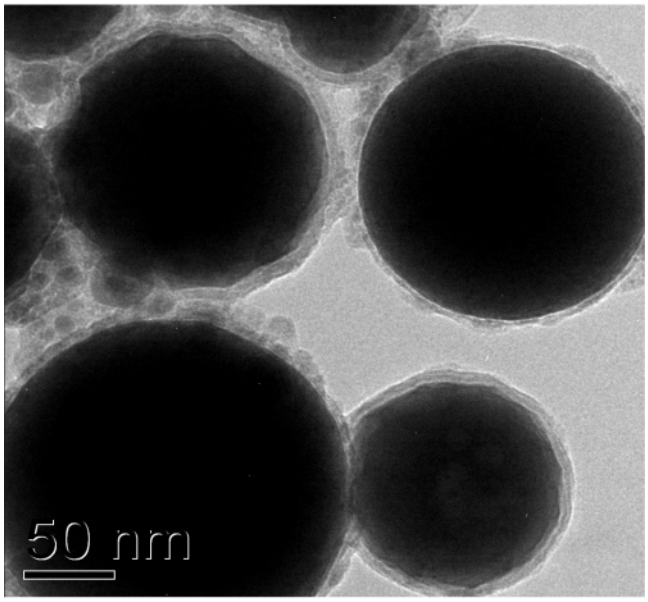

(b)

Figure 1. TEM images of the graphite-coated iron nanoparticles. (a) Wider scan showing the distribution of nanoaprticle sizes. (b) Zoom image showing the graphite coating on each of the iron core.

X-ray diffraction (XRD) analysis with a Siemens Powder XRD D5005 diffractometer also confirmed the formation of both graphite and iron phases by revealing the characteristic diffraction peaks of crystalline graphite and the iron bcc phase[16] (Figure 3). The XRD pattern is in agreement with the SAED image taken of the graphite-coated iron nanoparticles.

(16) Joint Committee on Standards, Powder Diffraction. *Diffraction Data File*; JCPDS Instrumental Center for Diffraction Data: Newtown Square, PA, 1991.

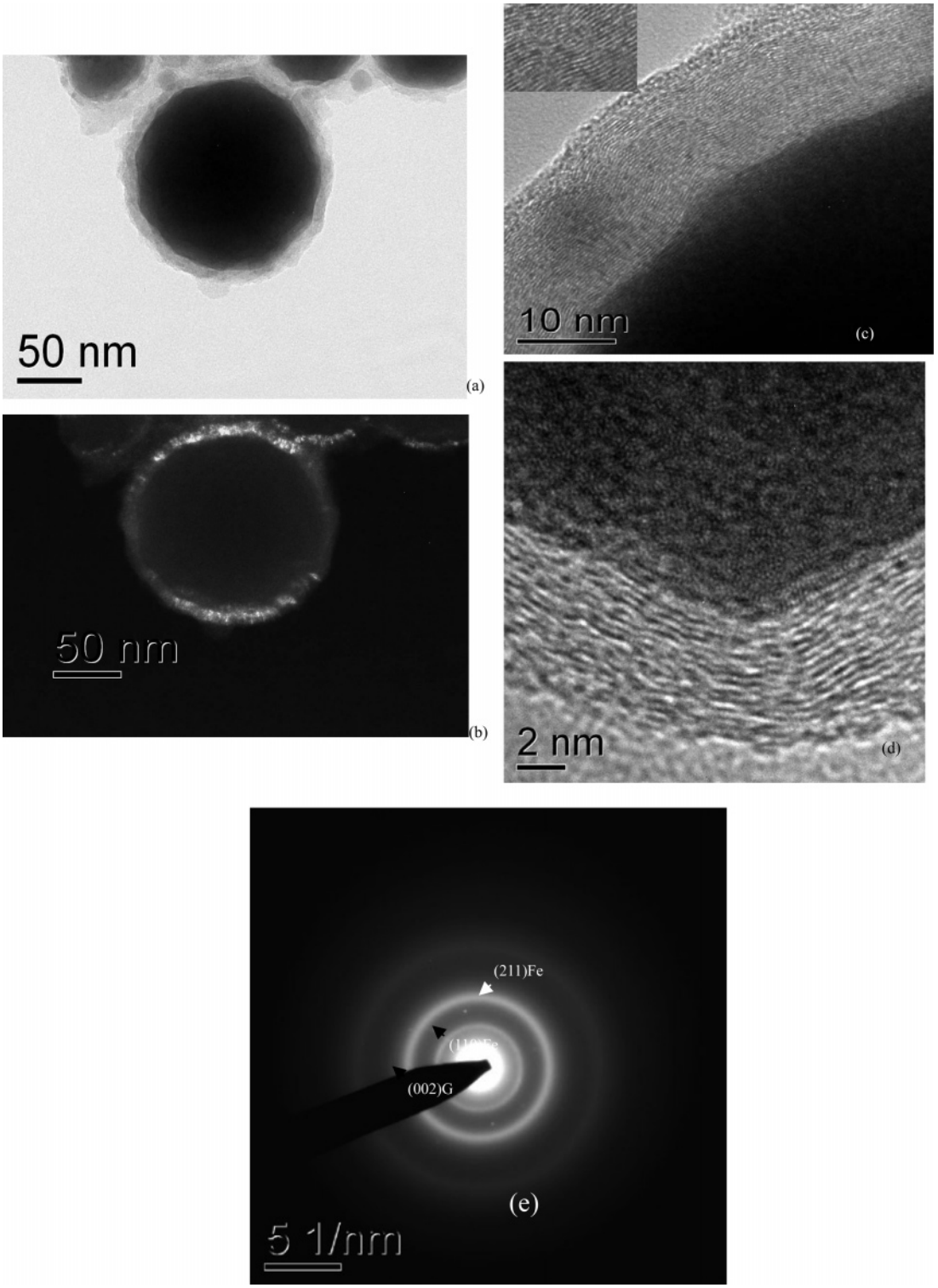

Figure 2. HRTEM images of the graphite-coated iron particles taken with JEOL TEM-3010 showing the clear graphite layer in (a) bright-field image and (b) dark-field image, (c) HRTEM image of the graphite shell, (d) HRTEM image of iron core (e) SAED of the core−shell nanostructure.

The confocal Raman spectrum (Renishaw inVia Raman microscope, $\lambda_{argon} = 514.5$ nm) of the graphite-coated iron particles in solid form was carried out to examine further the crystallinity of the graphite shell (Figure 4). In the Stokes Raman spectrum, two bands were recorded in which the first one centers at 1590 cm^{-1}. This band is attributed to the graphite crystallites G band; this band is inherent in the graphite lattices. More interestingly, the second band is at 1357 cm^{-1}, which is referred to as the main defect D1 band. According to the relationship between the D1/G intensity ratio and the graphite crystallinities,[17] we found that the inner layers of the graphite shells of our nanoparticles are highly crystalline but some defects are found on the outer layers.

The composition of the graphite-coated iron particles were examined by energy-dispersive X-ray spectroscopy (EDS)

(17) Wopenka, B.; Pasteris, J. D. *Am. Mineral.* **1993**, *78*, 533.

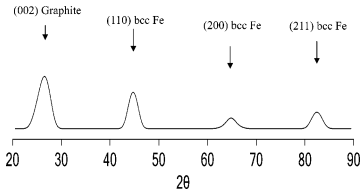

Figure 3. X-ray diffraction pattern (XRD) of the graphite-coated iron particles.

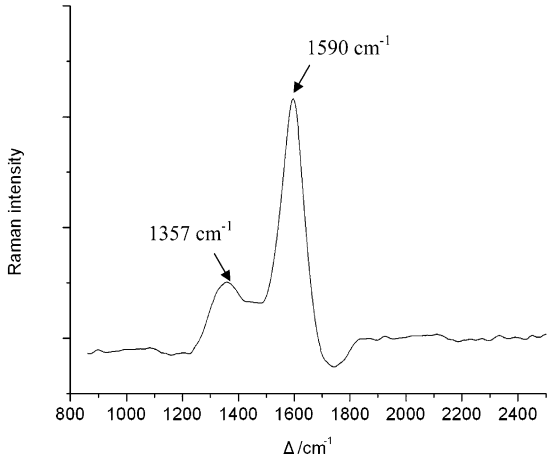

Figure 4. Confocal Raman spectrum of the graphite-coated iron particles. Both the G (1590 cm^{-1}) and D (1357 cm^{-1}) bands of graphite have been observed.

analysis. At the edge of the graphite-coated iron particle, it was found that the shells are composed almost entirely of carbon with an atomic percentage greater than 85%. On the other hand, the atomic percentage of Fe is much larger, greater than 80% in the core area. Note that even if the core is entirely composed of iron, some carbon signals would still be recorded, because the EDX beam has to pass through the graphite shell during the measurements. In both cases, no oxygen signal was observed, which may indicate the complete decomposition of the precursor [$Fe_3(CO)_{12}$] and the protection of the graphite layers against oxidation of the iron cores.

The graphite-coated iron nanoparticles were exposed to air for 22 days, after which they were analyzed by EDS once again. This time a little oxygen was detected in the shell only, while no any oxygen signal was observed in the core area. This result indicates that the inner layers of the graphite shell are highly crystalline, whereas the defects on the outer layers must have interacted with the oxygen species presumably adsorbed on the surface. Highly crystalline inner layers prevent oxygen from oxidizing the iron cores. In another experiment, the graphite-coated iron nanoparticles were dispersed in concentrated HNO_3 solution and aged for 4 days. From the TEM images (see the Supporting Information) taken of these particles, we found that almost none of the iron cores underwent reaction with acid. The two results presented here showed that highly stabilized graphite-coated iron nanoparticles have been obtained.

We have carried out further experiments as part of the study into the formation mechanism of the iron nanoparticles. We found that when oxygenated hexane solvent was used, only iron(II) oxide (FeO, confirmed by XRD, see the Supporting Information) particles were obtained without any

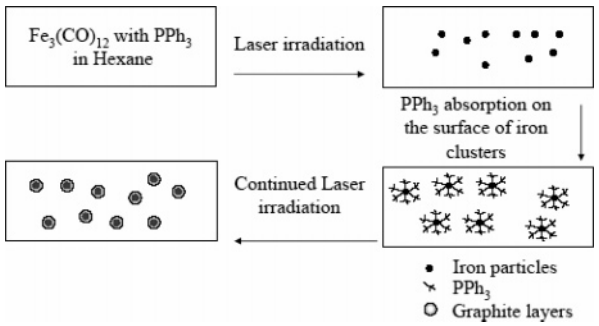

Figure 5. Proposed formation scheme of graphite-coated iron nanostructures.

graphitic shells around them. This shows that it takes only a little oxygen in the hexane solvent to oxidize the iron completely. Once the iron oxide formed, no graphitization can occur as well, because the oxidation of iron appears to proceed much faster than the graphitization on the surface of the iron nanoparticles. The same observation was seen even when phosphine was not added into the mixture. Hence, it is important to keep the solvent free from any oxidizing agent if iron nanoparticles were to be prepared. We have also investigated the origin of the graphite layers on the iron, because the carbon could come from either the phenyl ring of PPh_3 or from the solvent itself. We chose to use toluene as the solvent instead of hexane, because it can also provide an aromatic ring for graphitization; hence, a better comparison can be made. However, no graphite-coated iron nanoparticles were observed in deoxygenated toluene in the absence of PPh_3. Although the iron carbonyl precursor would still decompose under laser irradiation in toluene, the phenyl ring of toluene may not be close enough to the surface of the iron particles to initiate the graphitization process. Once PPh_3 was added to deoxygenated toluene, graphite layers were indeed formed. We attributed this occurrence to the adsorption or coordination between PPh_3 and iron, which allows the phenyl ring of PPh_3 to be sufficiently close to the iron surface for conversion to graphite.

In our case, the graphitization appears to have taken place under room-temperature conditions. However, an intense nanosecond pulse laser is well-known to provide the heat necessary for inducing molecular desorption on surfaces over a short period. Similarly, the laser energy could easily provide the heating effect for the graphitization process to occur at specific sites on the iron cores. Another important role provided by laser irradiation appears during the decomposition stage of the $Fe_3(CO)_{12}$ precursor. When a 200 W broadband xenon lamp ($300 < \lambda < 700$ nm) was used as the irradiation source instead, nanoparticles of any type could not be produced. This is presumably due to the inability of inducing complete iron carbonyl dissociation under much weaker irradiation. However, the intense pulse provided by the YAG laser ensures that any iron carbonyl intermediates formed will undergo further dissociation to form iron nanoparticles. In fact, it is well-known that in the light-induced homogeneous catalytic isomerization of alkenes in the presence of $Fe_3(CO)_{12}$ or $Fe(CO)_5$, many intermediates containing tricarbonyl or tetracarbonyl iron species are believed to be present in the mixture.[18] Under continuous

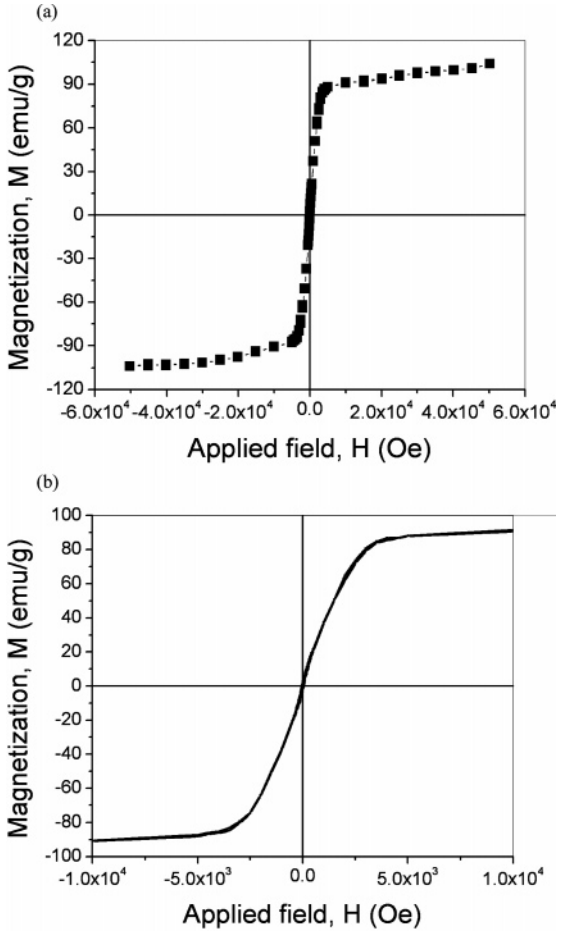

Figure 6. Magnetization measurement using SQUID (a) −5 to 5 T at 300 K, (b) zoom image from −1 to 1 T at 300 K.

and intense laser photolysis, these reactive intermediates would further decompose to yield $Fe(CO)_2$ or Fe(CO) and eventually Fe atom itself.[19]

On the basis of the experimental findings, we proposed a synthetic scheme (Figure 5) for the formation of the graphite-coated iron spheres. In the initial step, the precursor [$Fe_3(CO)_{12}$] was dissociated into Fe atoms and CO under intense laser photodecomposition. Free phosphines then began to adsorb onto the surface of the iron spheres. With continuous irradiation, the phenyl rings of the attached PPh_3 undergo graphitization and form the graphite layers around the iron cores.

The magnetic property of the iron nanoparticles was studied using a superconducting quantum interference device (SQUID). Figure 6 shows the field-dependent magnetization of the graphite-coated iron nanoparticles measured at 300 K. At this temperature, the magnetization of the sample can be completely saturated at high fields of up to 5 T. The magnetization at 5 T is 103.9 emu/g. The nonsaturated magnetization behaviors, the zero magnetic remanence, and the anhysteretic loop feature (more clearly seen in the field range of −1 to 1 T) indicates that the graphite-coated iron nanoparticles are superparamagnetic at room temperature. The superparamagnetic behavior of these graphite-coated iron nanoparticles corresponds well with the results of the TEM analysis in Figure 2, which revealed that the iron core possesses a polycrystalline structure with rather small grain size. The superparamagnetism of the assembly of nanosized grains have been observed and well-documented.[20] Recently, a number of approaches to making superparamagnetic particles as the magnetic contrast agents for magnetic resonance imaging (MRI) contrast enhancement have been developed.[21] A high magnetization value would certainly improve the magnetic contrast. Because the iron cores were coated with graphite shells, the shells provide an extremely effective barrier against oxygen, oxidizing agents, and even strong acids. The defects on the outer graphite layers make these magnetic particles easily functionalized[22] for possible biomedical applications.

Conclusion

Iron nanoparticles coated with graphite layers have been synthesized by 355 nm pulsed laser photodecomposition of triiron dodecacarbonyl $Fe_3(CO)_{12}$ in the presence of triphenylphosphine PPh_3. They have been shown to be stable toward oxygen and strong mineral acids. The graphite shell surrounding the iron core has been found to possess defects on its outer layers, hence providing suitable sites for functionalization. These superparamagnetic spherical nanoparticles also show a high magnetization value of 103.9 emu/g, as indicated by SQUID measurements.

Acknowledgment. We thank Lihui Van for the SQUID magnetic measurements. This work is carried out under an ASTAR nanoscience grant 143-000-198-305 and an NUS grant 143-000-298-112.

Supporting Information Available: EDX, XRD patterns, and TEM images. This material is available free of charge via the Internet at http://pubs.acs.org.

CM0706797

(18) (a) Mitchener, J. C.; Wrighton, M. S. *J. Am. Chem. Soc.* **1983**, *105*, 1065. (b) Mitchener, J. C.; Wrighton, M. S. *J. Am. Chem. Soc.* **1981**, *103*, 975. (c) Ouderkirk, A. J.; Wermer, P.; Schultz, N. J.; Weitz, E. *J. Am. Chem. Soc.* **1983**, *105*, 3354.

(19) (a) Tanaka, K.; Shirasaka, M.; Tanaka, T. *J. Chem. Phys.* **1997**, *106*, 6820. (b) Tanaka, K.; Sakaguchi, K.; Tanaka, T. *J. Chem. Phys.* **1997**, *106*, 2118.

(20) (a) Tartaj, P.; Serna, C. J. *J. Am. Chem. Soc.* **2003**, *125*, 15754. (b) Allia, P.; Coisson, M.; Tiberto, P.; Vinai, F.; Knobel, M.; Novak, M. A.; Nunes, W. C. *Phys. Rev. B* **2001**, *64*, 144420.

(21) (a) Berry, C. C.; Curtis, A. S. G *J. Phys. D* **2003**, *36*, R198. (b) Huh, Y.; Jun, Y.; Song, H.; Kim, S.; Choi, J.; Lee, J.; Yoon, S.; Kim, K.; Shin, J.; Suh, J.; Cheon, J. *J. Am. Chem. Soc.* **2005**, *127*, 12387.

(22) (a) Dai, H. *Acc. Chem. Res.* **2002**, *35*, 1035. (b) Tasis, D.; Tagmtarchis, N.; Bianco, A.; Prato, M. *Chem. Rev.* **2006**, *106*, 1105.